Received: 9 July 2019 | Revised: 5 August 2020 | Accepted: 10 August 2020

DOI: 10.1002/joc.6796

RESEARCH ARTICLE

International Journal of Climatology RMetS

Combined impacts of the El Niño-Southern Oscillation and Pacific Decadal Oscillation on global droughts assessed using the standardized precipitation evapotranspiration index

Phuong-Loan Nguyen[1] | **Seung-Ki Min**[2] | **Yeon-Hee Kim**[2]

[1]Climate Change Research Centre and ARC Centre of Excellence for Climate Extremes, UNSW, Sydney, NSW, Australia

[2]Division of Environmental Science and Engineering, Pohang University of Science and Technology, Pohang, South Korea

Correspondence
Seung-Ki Min, Division of Environmental Science and Engineering, Pohang University of Science and Technology, Pohang, South Korea.
Email: skmin@postech.ac.kr

Funding information
Korea Meteorological Administration, Grant/Award Number: KMI 2018-03610; National Research Foundation of Korea, Grant/Award Number: 2017R1A2B2008951

Abstract

Using the standardized precipitation evapotranspiration index, this study examines the combined effects of El Niño-Southern Oscillation (ENSO) and Pacific Decadal Oscillation (PDO) on global droughts in terms of magnitude, timing, and duration. The ENSO-affected drought hotspots are identified based on drought magnitude and probability of occurrence: five hotspots for El Niño (Amazon, India, central China, Indonesia, and eastern Australia) and four hotspots for La Niña (southeastern United States, southern South America, East Africa, and Southwest Asia). When ENSO and PDO are in phase, most of the hotspots exhibit an intensification and expansion of drought, more clearly at longer time scales (6–12 months), supporting previous studies. Interestingly, the in-phase PDO advances El Niño-induced drought onset by early summer of the previous year, whereas it delays the withdrawal of La Niña-induced drought until the end of the event year. This asymmetric response is found to be in part associated with the earlier start and later end of El Niño itself during warm PDO, which does not hold for the La Niña/cold PDO composites. Further analyses of the responses of precipitation (P) and potential evapotranspiration (PET) to different ENSO-PDO combinations suggest the important role of P reduction in determining drought magnitude and timing over most of the hotspots, with some contribution of enhanced PET to drier conditions over a few La Niña hotspots. It is also found that the PDO modulation of El Niño-induced drought occurs primarily through the eastern Pacific El Niño with a limited influence on the central Pacific El Niño.

KEYWORDS

combined effects, droughts, ENSO, PDO, SPEI

1 | INTRODUCTION

Drought is "a period of the abnormally dry weather long enough to cause a serious hydrological imbalance" as defined by the Intergovernmental Panel on Climate Change (IPCC, 2012). Since recent series of long-term droughts occurred over various parts of the world such as eastern Africa, southeastern Australia, western United States, and Argentina (Rivera and Penalba, 2014; Ficklin *et al.*, 2015; Ghebrezgabher *et al.*, 2016; McGree *et al.*, 2016), drought severity has gained wide attention. Meteorological drought is primarily controlled by the

 © 2020 Royal Meteorological Society

atmospheric circulation and ocean surface temperature (McCabe *et al*., 2004; Hoerling *et al*., 2006; Brönnimann, 2007; García-Herrera *et al*., 2007). The El Niño-Southern Oscillation (ENSO), an interannual fluctuation of warm (El Niño) and cold (La Niña) sea surface temperature (SST) conditions over the eastern equatorial Pacific, has been identified as a main driver of many drought episodes around the world (Trenberth *et al*., 2014). During El Niño events, drought was observed over southern United States and northern Mexico (Vicente-Serrano *et al*., 2011; Sun *et al*., 2016), South Africa (Rouault, 2005; Manatsa *et al*., 2015), Indonesia and Australia (Ashcroft *et al*., 2014; McGree *et al*., 2016), and Amazon (Zou *et al*., 2015; Jimenez-Munoz *et al*., 2016) as a result of shift of the main rainfall system in the tropical Pacific (Zhao *et al*., 2019). On the other hand, La Niña-related dry areas include southeastern United States (Okumura *et al*., 2017a), Chile (Quintana, 2000), East Africa (Coghlan, 2011), and El Niño-induced wetting places (Trenberth *et al*., 2014).

Recent studies showed that the ENSO teleconnection is not stationary and could be modulated by a decadal variability in Pacific SSTs, so called Pacific Decadal Oscillation (PDO) or the Interdecadal Pacific Oscillation (IPO) (Gershunov and Barnett, 1998; Yeh *et al*., 2018; Rao *et al*., 2019a). Generally, the positive (or warm) PDO favours more frequent and intense El Niño events while La Niña is fostered by the negative (or cold) PDO, overall intensifying ENSO teleconnection impacts on regional climate across the globe. For examples, the European winter rainfall and south China spring rainfall response to El Niño become stronger and more significant during the warm PDO phase than the cold PDO phase (Zanchettin *et al*., 2008; Xiao *et al*., 2015; Wu and Mao, 2016). Similarly, the impact of ENSO on Alaskan winter temperature is significantly different during positive and negative PDOs (Papineau, 2001).

PDO can modify the relationship between ENSO and regional climate extreme events like droughts though strengthening or weakening the ENSO-associated atmospheric circulation anomalies, increasing concerns about intensified drought responses at both global and regional scales. For example, the cold PDO may intensify a La Niña-induced negative Pacific/North America (PNA) pattern, leading to anomalous divergence of water vapour transport that favours dry conditions over the Great Plains, which becomes weaker during the warm PDO (Hu and Huang, 2009; Wang *et al*., 2014). By using both observations and model simulations, Krishnamurthy and Krishnamurthy (2013) suggested an increased occurrence of more intense drought over India when the warm PDO and El Niño co-occurred. The warm PDO strengthens the Walker and Hadley circulations in the equatorial Indian Ocean, leading to the enhancement of conventional monsoon-ENSO relationship. The connection between ENSO and PDO on East Asia climate has been also discussed in many literatures. Generally, combined El Niño and warm PDO configurations intensify the western North Pacific subtropical high, which transports warm and wet air into the East Asian continent, weakening East Asian winter monsoon (Wang *et al*., 2008; Kim *et al*., 2013). Similarly, Wu and Mao (2016, 2018) found that La Niña-induced spring time dry conditions over south China become stronger during the cold PDO.

The global extended work of Wang *et al*. (2014) showed the contrast in ENSO influences on dry-wet changes between the two phases of PDO by using the observed self-calibrated Palmer Drought Severity Index (sc_PDSI; Palmer, 1965; Wells *et al*., 2004). Generally, when El Niño coupled with the positive PDO, ENSO-induced dry/wet anomalies tend to strengthen with more severe droughts occupying larger areas compared with the negative PDO, notably over central China, Indonesia, northeastern Australia, northern North America, northern South America, and southern Africa. The same situation was found for the La Niña-negative PDO combinations over southeastern United States and northern Mexico. During their out-of-phase combinations, the associated below-normal anomalies of sc_PDSI were weakened or even disappeared in many regions.

Drought is a multi-scalar extreme phenomenon and the time scale over which the precipitation deficits accumulate is important. The response of hydrological systems to precipitation changes also varies by time and can be affected by different climatic variables (McKee *et al*., 1993). In particular, vegetation and water resources exhibit different sensitivity to drought time scales, which determines differences between different drought types and impacts (e.g., López-Moreno *et al*., 2013; Vicente-Serrano *et al*., 2013; Barker *et al*., 2016; Peña-Gallardo *et al*., 2019). For this reason, considering drought under different time scales is necessary for water resource management. However, previous studies on the ENSO-PDO combined impacts on droughts have limitedly considered different time scales. By using a multi-scalar drought index of standardized precipitation evapotranspiration index (SPEI, Vicente-Serrano *et al*., 2010), the present study explores the changes in ENSO-induced drought characteristics including magnitude, duration, and timing under different PDO conditions. We also explore the possible physical mechanisms behind the modulations of regional ENSO-droughts relationship by PDO through analysing SST patterns and the relative contribution of precipitation and potential evapotranspiration to regional drought evolutions.

2 | DATA AND METHODS

2.1 | ENSO and PDO indices

We calculated the ENSO and PDO indices using HadISST v1.1 (Hadley Centre Global Sea Ice and SST; Rayner *et al*., 2003) SST dataset which covers the period 1870–2019. As an indicator of the ENSO variability, Niño 3.4 (5°S–5°N and 170°–120°W) index was calculated for 1901–2015 as area-mean monthly SST anomalies with respect to the 1961–1990 climatology. Niño 3 (5°S–5°N and 150°–90°W) and Niño 4 (5°S–5°N and 160°E–120°W) indices were also used for considering different El Niño types (see below). All ENSO indices were detrended prior to analysis to remove possible influence of long-tern trends although a weak positive trend is statistically insignificant. Considering that the ENSO amplitude is strongest with the largest SST anomalies during the boreal winter months (December to February, DJF), we use DJF mean ENSO indices. El Niño and La Niña events are defined when the detrended DJF Niño3.4 index exceeds ±0.6°C (0.8 *SD*s) following Gershunov and Barnett (1998) and Wang *et al*. (2014). Figure 1a displays the Niño3.4 index and selected ENSO events.

To consider ENSO flavours, El Niño events are further divided into eastern Pacific El Niño (EP) and central Pacific (CP) El Niño following Yeh *et al*. (2009). El Niño events which have Niño 3 index larger than the Niño 4 index are classified into EP El Niño while CP El Niño events are characterized by the Niño 4 index larger than the Niño 3 index (Table 1). CP El Niño events have not occurred before the 1950s, so we focus on the recent period 1950–2015 when comparing EP and CP El Niño events.

We calculated the PDO index following Mantua *et al*. (1997) as the time series of the first empirical orthogonal function mode of SST anomalies in the North Pacific Ocean (poleward of 20°N). Monthly global mean SST anomaly was subtracted at each grid point before analysis to exclude the possible influence of global warming. Monthly PDO index was then averaged over

TABLE 1 Classification of years based on the phase of ENSO and PDO for the 1901–2015 period

	Warm PDO	Cold PDO
El Niño	1903, 1905, 1906, 1924, 1926, 1931, 1940, 1941, 1942, 1978, 1983, 1987, 1988, 1992, 1995, 1998	1912, 1914, 1915, 1919, 1958, 1964, 1966, 1969, 1973, 1977, 2003, 2010, 2015
La Niña	1904, 1909, 1910, 1925, 1934, 1939, 1943, 1984, 1985, 1986, 1989, 1996, 1999, 2000, 2001	1917, 1918, 1950, 1951, 1955, 1956, 1965, 1971, 1974, 1976, 2006, 2008, 2009, 2011, 2012

Note: The year indicates the year of January and February (i.e., 1903 refers to the boreal 1902–1903 winter). Underlines denote Central Pacific El Niño events.

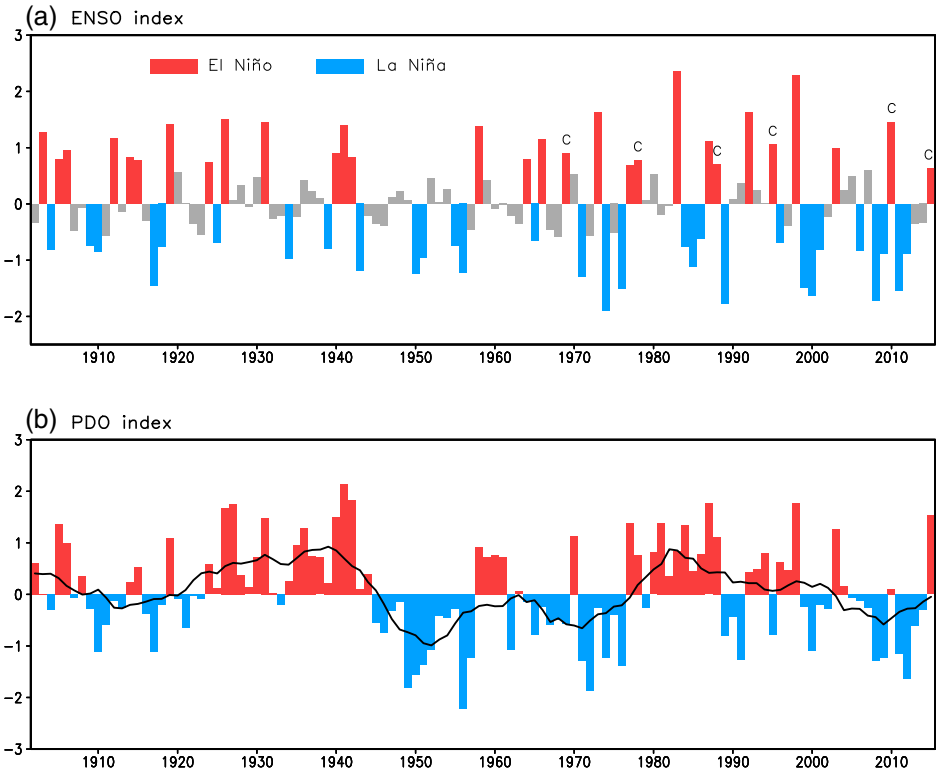

FIGURE 1 (a) ENSO events (El Niño in red and La Niña in blue; "c" denote Central Pacific El Niño) defined from detrended Niño3.4 SST index averaged for December–February and (b) PDO phases (warm PDO in red and cold PDO in blue) defined from November–March averaged PDO index. The black-solid line indicates 11-year running means and the corresponding 2015 value is calculated from nine-year average (2011–2019) due to data limitation [Colour figure can be viewed at wileyonlinelibrary.com]

each extended winter season (November to March, NDJFM) following Wang *et al*. (2014). In order to retain interdecadal variability of PDO index, an 11-year running mean was applied and the warm and cold PDO phases were defined based on its sign (Figure 1b). There are three warm PDO epochs (1902–1910, 1921–1945, and 1978–2002) and three cold PDO epochs (1911–1920, 1946–1977, and 2003–2015).

Although the temporal correlation coefficient (r) between the Niño 3.4 index and the unfiltered PDO is 0.59 during 1902–2015, exceeding a 5% significance level, the 11-year running mean of PDO index is scarcely related to the Niño 3.4 index ($r = .15$), suggesting the overall distinction between the interannual ENSO variability and the decadal variation of PDO index. Finally, ENSO events are categorized into four groups based on whether the ENSO events belong to the warm or cold PDO epochs (Table 1). The years listed in Table 1 correspond to those from January and February. Note that ENSO and PDO events classified here are overall similar to previous studies (e.g., Wang *et al*., 2014; Rao *et al*., 2019b) but small differences exist, which seem to be due to the differences in data, analysis period, and/or definition of events across studies.

2.2 | SPEI

The SPEI is utilized to characterize drought fluctuations over the study areas, and its standardized nature allows efficient comparisons of droughts between different regions having different climatology conditions. In addition, SPEI calculation is based on the difference in precipitation (P) and potential evapotranspiration (PET), and thereby effectively considers changes in atmospheric evaporative demand (Vicente-Serrano *et al*., 2010, 2020). To quantify the changes in drought characteristics, we used the SPEI dataset v2.5 available from the Global SPEI database (Vicente-Serrano *et al*., 2010; https://spei.csic.es/index.html). This SPEI dataset was constructed based on the accumulative climatic water balance, that is, difference between monthly P and PET, at different time scales (1–12 months) using Climate Research Unit dataset (CRU TS 3.24.01, Harris *et al*., 2014) with spatial resolution of $0.5^\circ \times 0.5^\circ$ for 1901–2015 period. The accumulative water balance fits into log-logistic distribution to transform to standardized units. The time scales here mean the accumulation months for P and PET. For example, 12-month SPEI (SPEI12) for December 1901 is calculated from accumulative P and PET from January 1901 to December 1901. More detailed information on SPEI data and its calculation are referred to Vicente-Serrano *et al*. (2010). Drought can occur from decrease in P, increase in PET, or both. To assess the relative contribution of P and PET to SPEI responses, we use P and PET data from CRU TS (version 3.24.01) for the same period (for details of PET calculation, refer to Appendix 1 of Harris *et al*., 2014). Anomalies are made relative to the whole period mean of 1901–2015. For all variables, the linear trend was removed (detrended) before analysis to remove the possible effects of global warming.

Recently, atmospheric evaporative demand (AED) is recommended to be used instead of PET, which is an umbrella term that introduces different concepts such as the reference evapotranspiration, the open water evaporation, and the pan evaporation (Vicente-Serrano *et al*., 2020). However, considering that PET has been a long-established hydrological variable and often used interchangeably with AED (e.g., Peng *et al*., 2018), here we keep using PET for consistency with previous studies (Vicente-Serrano *et al*., 2011; Harris *et al*., 2014). Drought concepts in deserts, hyper-arid and cold areas might be physically meaningless (Carrao *et al*., 2014; Spinoni *et al*., 2014). We utilize the global aridity index dataset from Spinoni *et al*. (2014) to exclude these regions from our analysis. Hereafter, the term of "global land" refers to the land areas all around the world except deserts, hyper-arid and cold areas.

2.3 | Drought hotspots and composite analyses

To examine ENSO and PDO influences on global and regional droughts, drought hotspots were selected as areas that have significantly dry conditions during boreal winters (DJF). SPEI12 was used because 12-month accumulative period is more preferable to demonstrate annual drought patterns than shorter time scales (Vicente-Serrano *et al*., 2010; Spinoni *et al*., 2014). In addition, SPEI12 shows maximum spatial correlation with the sc_PDSI (figure 12 of Vicente-Serrano *et al*., 2010), enabling better comparisons with previous studies (Wang *et al*., 2014). We require two conditions for drought hotspots. First, SPEI value is below −1 ("moderate" drought), corresponding to about 15th percentile of the normal distribution of SPEI values (Vicente-Serrano *et al*., 2011). Second, area-mean drought probability is above 25%, which is defined as the number of months with SPEI ≤ -1 divided by total ENSO months. Figure 2 illustrates the spatial distribution of the drought probability and the boreal winter mean SPEI12 composites for El Niño and La Niña events. Based on these composites of drought probability and severity, we select nine drought hotspots (Table 2): five hotspots for El Niño (Amazon, India, central China, Indonesia, and eastern Australia)

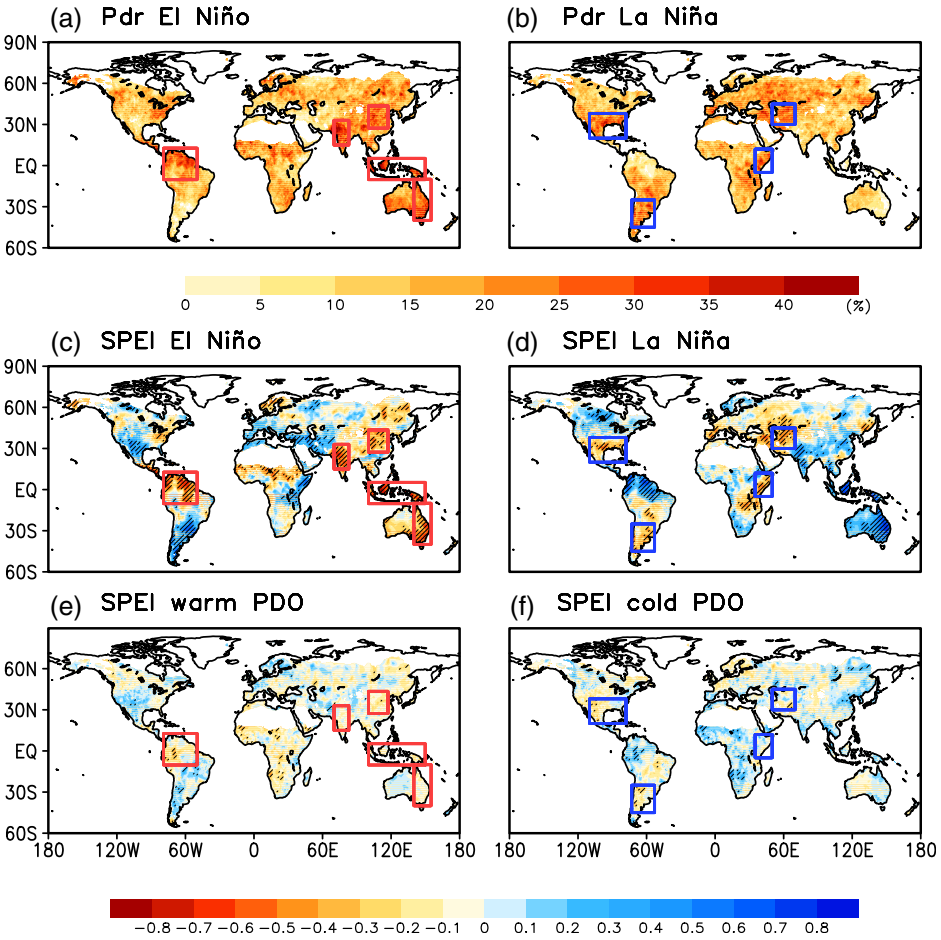

FIGURE 2 Spatial distribution of the probability of drought conditions (Pdr, SPEI12 ≤ −1) during (a) El Niño and (b) La Niña events. Composite of the DJF detrended SPEI12 for 1901–2015 period for (c) El Niño, (d) La Niña, (e) warm PDO, and (f) cold PDO. The hatching indicates significant results at 10% level according to a two-tailed Student's *t*-test. The red and blue open boxes indicate El Niño and La Niña drought hotspots (see Table 2 for longitude-latitude ranges) [Colour figure can be viewed at wileyonlinelibrary.com]

TABLE 2 Drought hotspots (land only) selected for El Niño and La Niña

ENSO phase	Region	Longitude	Latitude
El Niño hotspots	Amazon	79.25 W–49.75 W	10.25 S–12.75 N
	India	70.25 E–85.25 E	15.25 N–33.25 N
	Central China	100.25 E–117.25 E	27.25 N–43.25 N
	Indonesia	100.25 E–149.75 E	10.25 S–5.25 N
	Eastern Australia	139.75 E–154.75 E	40.25 S–10.75 S
La Niña hotspots	Southeastern United States	110.25 W–78.25 W	20.25 N–38.75 N
	Southern South America	63.25 W–53.25 W	40.25S–25.25S
	East Africa	35.25 E–50.25 E	5.25S–7.25 N
	Southwest Asia	50.25 E–70.25 E	30.25 N–45.25 N

and four hotspots for La Niña (southeastern United States, southern South America, East Africa, and Southwest Asia).

It is generally accepted that PDO modulates ENSO-drought relationship (Gershunov and Barnett, 1998; Wang *et al*., 2008; Hong *et al*., 2013; Wang *et al*., 2014). However, other studies suggest the different physical linkage between ENSO and PDO at both interannual and decadal time scales (Newman *et al*., 2003; Schneider and Cornuelle, 2005; Newman *et al*., 2016; Wu and Mao, 2016, 2017). To consider the possible ENSO-PDO dependence, we conducted a sensitivity test to the use of independent indices of ENSO and PDO, which was obtained based on a simple linear regression of one index onto the other index (e.g., regression of Niño3.4 index onto PDO index). Although there are some changes in La Niña drought hotspots, the main results were found to be largely insensitive the use of the independent indices (Figure S1). As suggested by Gershunov and Barnett (1998) and Rao *et al*. (2019a), the term

"modulation" used in this study means that PDO can affect ENSO-related climate signals over drought hotspots.

To examine PDO modulation effects on ENSO-induced droughts, the global patterns of SPEI12 composites were constructed for four different ENSO-PDO combinations. To determine whether the SPEI values between in-phase and out-of-phase ENSO-PDO combinations are significantly different, a two-tailed Student's *t*-test was applied with 10% significance following Wang *et al*. (2014). Sub-sampled SPEIs for different ENSO-PDO combinations found to be normally distributed based on the Shapiro–Wilk test (not shown). Regional mean SPEIs for nine ENSO drought hotspots were then analysed to assess the changes in magnitude, timing and duration of droughts according to the different PDO phases. In particular, 1–12 month SPEIs were considered to examine the time scales of ENSO-PDO combined effects on droughts.

3 | RESULTS AND DISCUSSION

3.1 | ENSO-PDO impacts on global drought patterns

Before exploring the combined impacts of ENSO-PDO on global drought severity, the influence of individual climate variability is analysed. Composites of the DJF detrended SPEI12 for El Niño and La Niña events (Figure 2c,d) show that during boreal winter time, El Niño induces significant drying conditions over many parts of the world including the five El Niño hotspots and other regions like southern Australia, Alaska, and the Sahel. On the other hand, significant negative SPEIs are prominent over four La Niña hotspots. These are consistent with previous studies (Andreoli and Kayano, 2005; Pavia *et al*., 2006; Hu and Huang, 2009; Hoell *et al*., 2014; Wang *et al*., 2014; Barlow *et al*., 2016; Penalba and Rivera, 2016; Wu and Mao, 2017).

Composites of SPEI12 for warm and cold PDO epochs (Figure 2e,f) exhibit similar spatial patterns to those for ENSO but with weaker amplitudes. The warm PDO is characterized by significant negative SPEI anomalies over Amazon, the sub-Sahara regions, northeastern China and Siberia, but not clearly over Indonesia and eastern Australia. Cold PDO phases induce dry conditions over the southwestern United States and the southern South America, but the signals are much weaker over East Africa and Southwest Asia. The overall similar patterns between ENSO and PDO composites suggest that both climate variabilities may exert stronger drying impacts on similar parts of the world when they are in phase and vice versa.

Figure 3 shows the spatial distribution of SPEI12 composites for four ENSO-PDO combination (El Niño/warm PDO, El Niño/cold PDO, La Niña/warm PDO, and La Niña/cold PDO) constructed using the selected years listed in Table 1. The composite differences between different PDO phases (in-phase minus out-of-phase) are also illustrated for El Niño and La Niña, respectively, to isolate the influences of PDO. El Niño-induced droughts exhibit significant differences between the different phases of PDO (Figure 3a,b). Evidently, El Niño/warm PDO composites of SPEI12 feature substantially amplified negative SPEIs over many regions (Figure 3a), occupying larger areas of significant changes than those for El Niño/cold PDO composites (Figure 3c). In particular, intense dry conditions are observed over all five El Niño hotspots during warm PDO phases (Figure 3a), consistent with Wang *et al*. (2014). In addition, the spatial correlation of SPEI patterns between the case of El Niño/warm PDO with the canonical ENSO-induced pattern (Figure 2c) was very high as 0.86. During the cold PDO phase, El Niño-induced SPEI response becomes much weaker (Figure 3c), resulting in lower spatial correlation with the canonical pattern ($r = .80$). It is noticeable that over 15.3% of global land suffers significant dryness conditions (SPEI12 < 0 with $p < .1$) when El Niño occurs in warm PDO phases, which is greater than 12.5% from the El Niño/cold PDO combination. This indicates the dominant role of warm PDO winters in determining El Niño-induced global drought patterns. Composite differences between El Niño/warm PDO and El Niño/cold PDO (Figure 3e) illustrate that warm PDO enhances the El Niño-induced drought severity over central China and Amazon.

Two sub-composites for La Niña also show significant differences in La Niña-induced drought severity between the positive and negative PDO phases. When La Niña takes place in the cold PDO, strong negative SPEI was observed over the four La Niña drought hotspots (Figure 3d). During the warm PDO, however, the droughts become weaker and less organized (Figure 3b). La Niña-related negative SPEI values over southeastern United States, southern South America, and Southwest Asia almost disappeared, as can be seen from the composite difference pattern (Figure 3f). On the other hand, droughts over East Africa are relatively insensitive to the PDO phase. As in the El Niño case, the SPEI pattern for La Niña with the cold PDO has higher spatial correlation ($r = .88$) with the canonical composite (Figure 2d) than that with the warm PDO ($r = .76$). Similarly, the area fraction of world land with significant negative SPEI corresponding to La Niña in cold PDO and warm PDO is 9.5 and 5.7%, respectively, suggesting considerable contribution of PDO on La Niña-induced drought patterns.

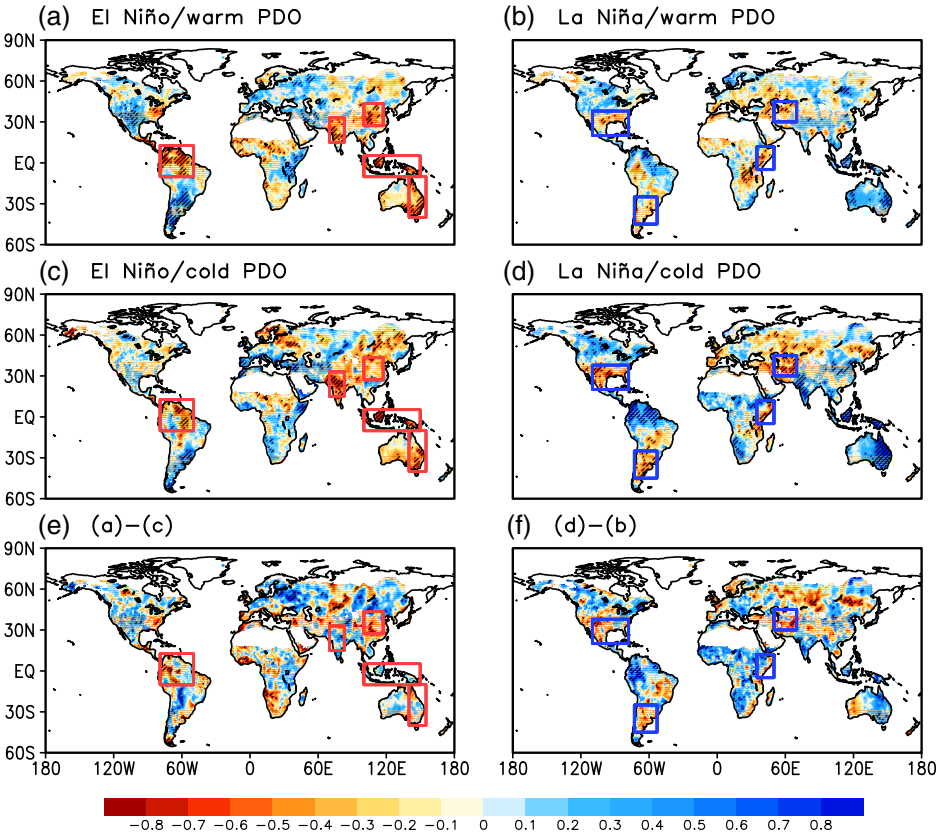

FIGURE 3 Composite patterns of DJF detrended SPEI12 for (a) El Niño/warm PDO, (b) La Niña/warm PDO, (c) El Niño/cold PDO and (d) La Niña/cold PDO and their differences (e) (a) – (c) and (f) (d) – (b). The hatching indicates significant responses or differences a 10% level according to a two-tailed Student's *t*-test [Colour figure can be viewed at wileyonlinelibrary.com]

When considering 3-, 6-, or 9-month time scales (Figures S2, S3, and S4), SPEI composites show similar results of intensified droughts when ENSO and PDO are in phases, indicating the robust PDO modulation of ENSO-induced drought teleconnections.

3.2 | ENSO-PDO impacts on regional drought characteristics

The modulation effect of PDO is further analysed with considering different time scales of droughts. By examining SPEI at 1–12 month time scales during ENSO, Vicente-Serrano *et al.* (2011) pointed out that "drought starts to emerge at short time scale and becomes more evident at longer time scales." This means that the drought that develops over short periods contributes to that at longer time scales. Using the same approach, we analyse drought magnitude, timing and duration during the 24 months of ENSO events (from January of the preceding year to December of the event year) under different PDO conditions. Figure 4 shows the evolutions of SPEI composites (ENSO event months in x-axis and drought time scale in y-axis) for the El Niño-induced and La Niña-induced droughts according to different PDO phases, where SPEIs are averaged over the corresponding El Niño and La Niña hotspots. The drought durations are identified when regional averaged SPEI falls below −0.2 (black dashed contour) and −0.4 (black solid contour). Note that we use smaller thresholds here to identify dry conditions based on regional averaged SPEIs. A simple comparison indicates that regional mean SPEI of 0.2 corresponds to sub-regional (drier half) mean of 0.84, which represents the return period of one in 5 years (see below). Overall, intense droughts are observed at longer time scales although there are considerable differences across hotspots (see Figures S5 and S6 for individual hotspots).

When ENSO is in phase with PDO, all drought hotspots share the similar feature of either earlier onset or later withdrawal, resulting in the lengthening of drought duration. For example, when El Niño occurs with warm PDO, significant negative SPEI is initially recorded from June of the previous year throughout 1–12 month time scales and its signal gets stronger at longer time scales, keeping dry conditions up to next summer of El Niño year (Figure 4a). In contrast, when El Niño is combined with cold PDO, dry conditions begin later around September of the previous year and ends earlier around July of the event year, based on SPEI12 (Figure 4c). This feature is commonly seen over all El Niño drought hotspots (Figure S5) with a couple of exceptions over Amazon where El Niño-induced dry condition begins with the El Niño event and last for several months and over India where the opposite pattern is observed.

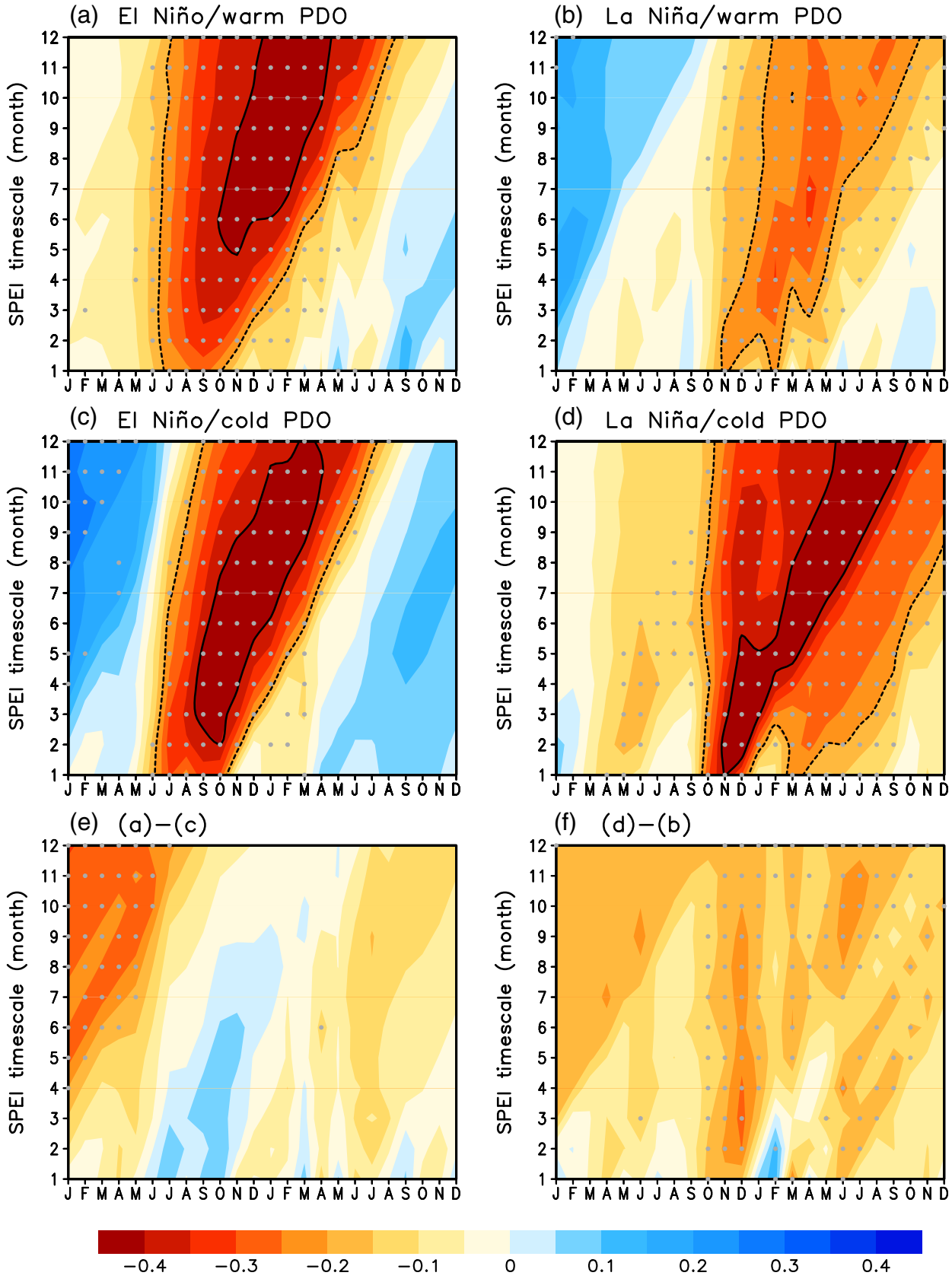

FIGURE 4 Composites of SPEI at 1–12 month time scales (y-axis) during 24 months of the ENSO event (x-axis) with different PDO phases, averaged over drought hotspots during (a) El Niño/warm PDO, (b) La Niña/warm PDO, (c) El Niño/cold PDO, (d) La Niña/cold PDO years, and their differences (e and f). Black solid and dashed contours indicate SPEI values of −0.4 and −0.2, respectively. The grey dots depict significant differences at 10% level according to a two-tailed Student's *t*-test [Colour figure can be viewed at wileyonlinelibrary.com]

Similar intensification and weakening of droughts are observed for La Niña years under cold and warm PDO phase, respectively, but different timing of droughts is noticeable (Figure 4b,d). During the in-phase combination (cold PDO), drought begins to emerge around September of the previous year at 1–3 month time scales and lasts until the end of La Niña year (Figure 4d). During the warm PDO, however, La Niña-induced droughts become much weaker with short duration of a few months (Figure 4d), consistent with global patterns described above (Figure 3b). In this case, drought events almost disappear in southern South America (Figure S6). In addition, it is notable that strongest droughts (SPEI < −0.4) occur during the summer (June–August) of La Niña years whereas strongest droughts are seen during the winter (January–March) of El Niño years, which seems to be partly related to the different evolution and duration of SST anomalies over the equatorial Pacific between ENSO phases (see below).

Drought onset and withdrawal are further compared using SPEI12 between the different PDO polarities for all hotspot average (ALL) and each hotspot (Figure 5). Regional mean SPEI values of −0.2 and −0.4 as well as drier half sub-regional mean SPEI of −0.84 are used to indicate drought duration. As analysed above, ALL results show that when ENSO occurs in phase with PDO, earlier drought signal is detected from summer (July for El Niño) or autumn (October for La Niña) of the previous year and persisted over about 1 year. However, the regional analyses reveal large differences in the drought timing and duration and the degree of PDO influences. When El Niño is combined with the warm PDO, negative SPEI value emerges from July to September of the previous year over four hot spots (except Amazon). Over Amazon, strong negative SPEI12 is recorded from February of the El Niño winter and lasts until the September. In contrast, under out-of-phase conditions, the drying impacts are identified later with shorter duration over all hotspots except India. For example, El Niño effects on drought start in September over Indonesia. Greater shortening of El Niño-induced drought is observed in central China and Amazon.

On average, the PDO modulation impacts on drought onset and withdrawal are more evident for La Niña than

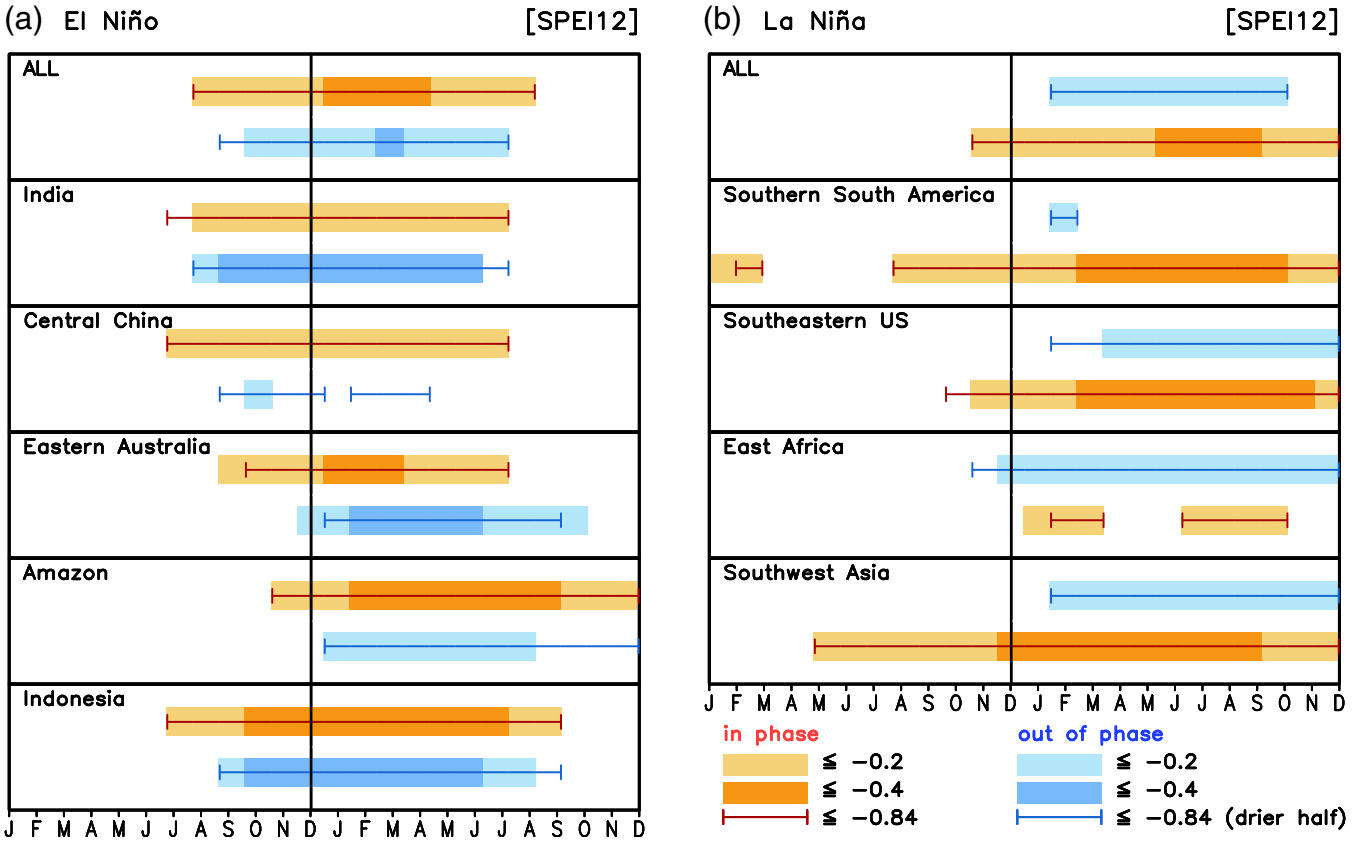

FIGURE 5 Comparisons of ENSO-induced drought timing and duration for SPEI12 during (a) El Niño and (b) La Niña. Years in phase (reddish colour) and out of phase (bluish colour) with PDO are compared for all hotspot averages (ALL) and individual hotspots. Light and dark filled bars indicate months with area-averaged SPEI12 below −0.2 and −0.4, respectively. Error bars represent months with sub-regional (dry half) mean SPEI12 below −0.84. See text for details [Colour figure can be viewed at wileyonlinelibrary.com]

for El Niño (Figure 5b). ALL results show that when La Niña occurs during the cold PDO, drought condition is detected over longer than one year, but it is shortened to several months with weaker strength when La Niña occurs during the warm PDO. Warm PDO shortens the drought period over all hotspots except East Africa, in particular, with almost no drought occurring over southern South America. Analyses considering 3-month, 6-month, and 9-month SPEIs provide similar results to those from SPEI12 (Figures S7, S8, and S9). A noticeable difference is that earlier onset of drought is observed for 3-month SPEI particularly over India, eastern Australia, Indonesia, and southern South America, indicating its short time-scale response to El Niño (Vicente-Serrano *et al*., 2011). Overall, the in-phase PDO tends to delay the withdrawal of La Niña-induced drought whereas it rather advances the onset of El Niño-induced droughts, causes of which is discussed below.

3.3 | Mechanisms for drought responses

ENSO is the primary source of variability in the tropical precipitation (Gu *et al*., 2007; Trenberth *et al*., 2014) whereas over mid-high latitudes ENSO-induced effects arise often through atmospheric teleconnections (Trenberth and Hoar, 1997; Diaz *et al*., 2001; Rao and Ren, 2017, 2018; Stan *et al*., 2017). ENSO teleconnections lead to different regional responses of precipitation and temperature, and thus impose different changes in regional drought conditions as well (Trenberth *et al*., 2002; Sen Roy *et al*., 2003; Dai *et al*., 2015). For the same reason, the modulation of the ENSO teleconnections by different PDO phases can be different between ENSO phases and among drought hotspots.

In this section, we discuss the possible reasons for the asymmetric response of El Niño and La Niña-related droughts to different PDO phases. One possible cause is the different SST anomaly evolutions between El Niño and La Niña events. To check this, we examine the monthly evolution of Niño3.4 index anomalies during El Niño and La Niña events for the different phases of PDO (Figure 6). El Niño onset is characterized by positive SST anomalies over eastern equatorial Pacific exceeding 0.8 *SD* (~0.6°C, Figure 6a). During the warm PDO (red line), the significant positive SST anomalies are observed from late spring of May and rapidly intensified. El Niño onset is recorded in July of the previous year and reaches its peak during winter season. During the peak El Niño, this warmer than normal SST is not only amplified but also expanded meridionally (Rao *et al*., 2019a, 2019b). This SST intensification occurs because ENSO and PDO induce a similar background SST anomaly distribution with the same sign of positive SST anomalies over equatorial Pacific and negative SST anomalies over mid latitude North Pacific (Namias *et al*., 1988; Gershunov and

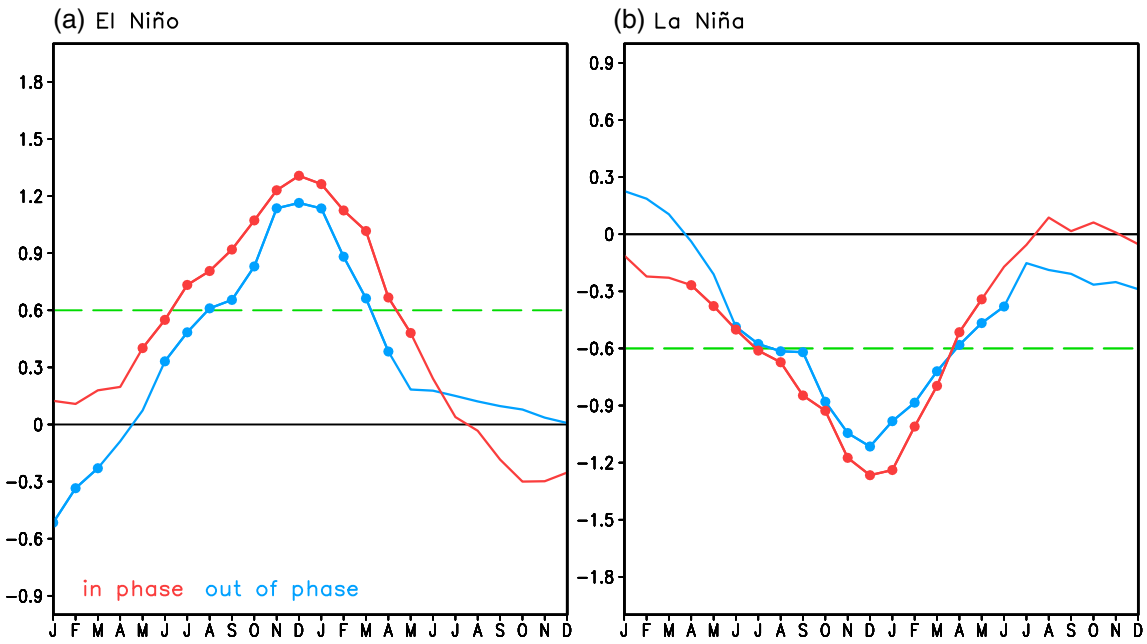

FIGURE 6 Composite evolution of the Niño3.4 index (°C) during the 24-month period of (a) El Niño and (b) La Niña for the in-phase (red) and out-of-phase combinations (blue) with PDO. The horizontal dashed (green) lines indicate +0.6°C for El Niño and −0.6°C for La Niña, which are used to identify ENSO duration. The dot marks represent statistically significant Niño3.4 values at 10% level [Colour figure can be viewed at wileyonlinelibrary.com]

Barnett, 1998). On the other hand, offsetting effect of negative background SST anomalies from the cold PDO delays El Niño onsets (August) and also weakens the warmer SST along the equator. In addition, noticeable differences in SST amplitudes between the in-phase and out-of-phase combinations are observed from the beginning of El Niño event to the next March, explaining in part the longer duration of El Niño-induced droughts during in-phase PDO conditions (Figure 5a). This earlier start and later end of El Niño during the warm PDO are in line with the recent finding of Okumura *et al*. (2017b).

The La Niña-related SST amplitude also exhibits a similar difference but not striking as in the El Niño cases (Figure 6b). In La Niña/cold PDO composites, significant negative SST anomalies are recorded at early spring of previous year, which is 2-month earlier than those during warm PDO phases, and then rapidly enlarge. During the peak season, spatial expansion and intensification of significant negative SST anomalies are also observed over tropical Pacific (not shown). However, there is no systematic difference in the timing and duration of La Niña events associated with the PDO polarity, emerging from August of the previous year, reaching its peak in December, and decaying to the next April.

Asymmetric response of ENSO characteristics under the two phases of PDO can lead to asymmetric

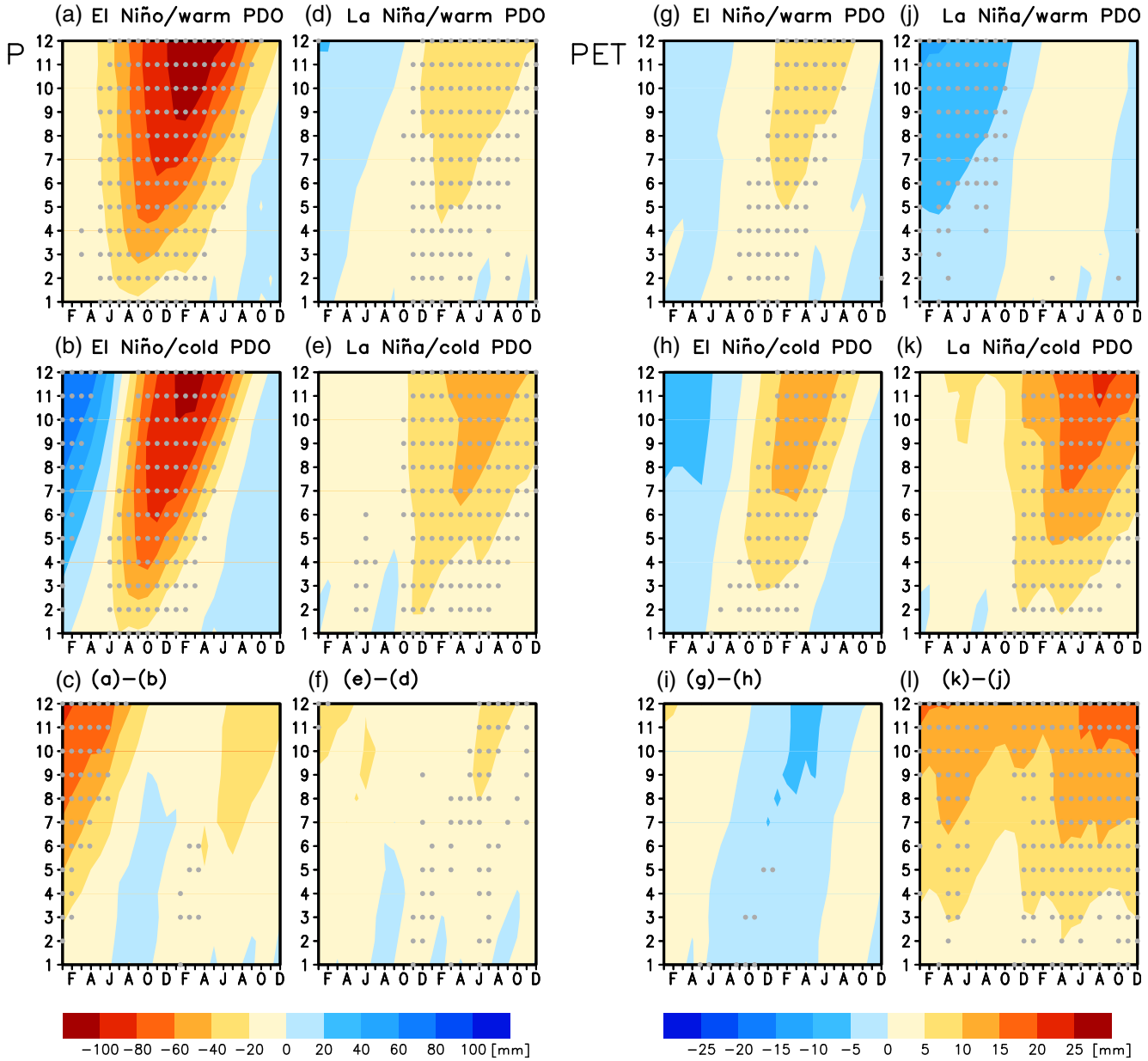

FIGURE 7 Same as Figure 4 but for precipitation (P, left) and potential evapotranspiration (PET, right). Note different scales [Colour figure can be viewed at wileyonlinelibrary.com]

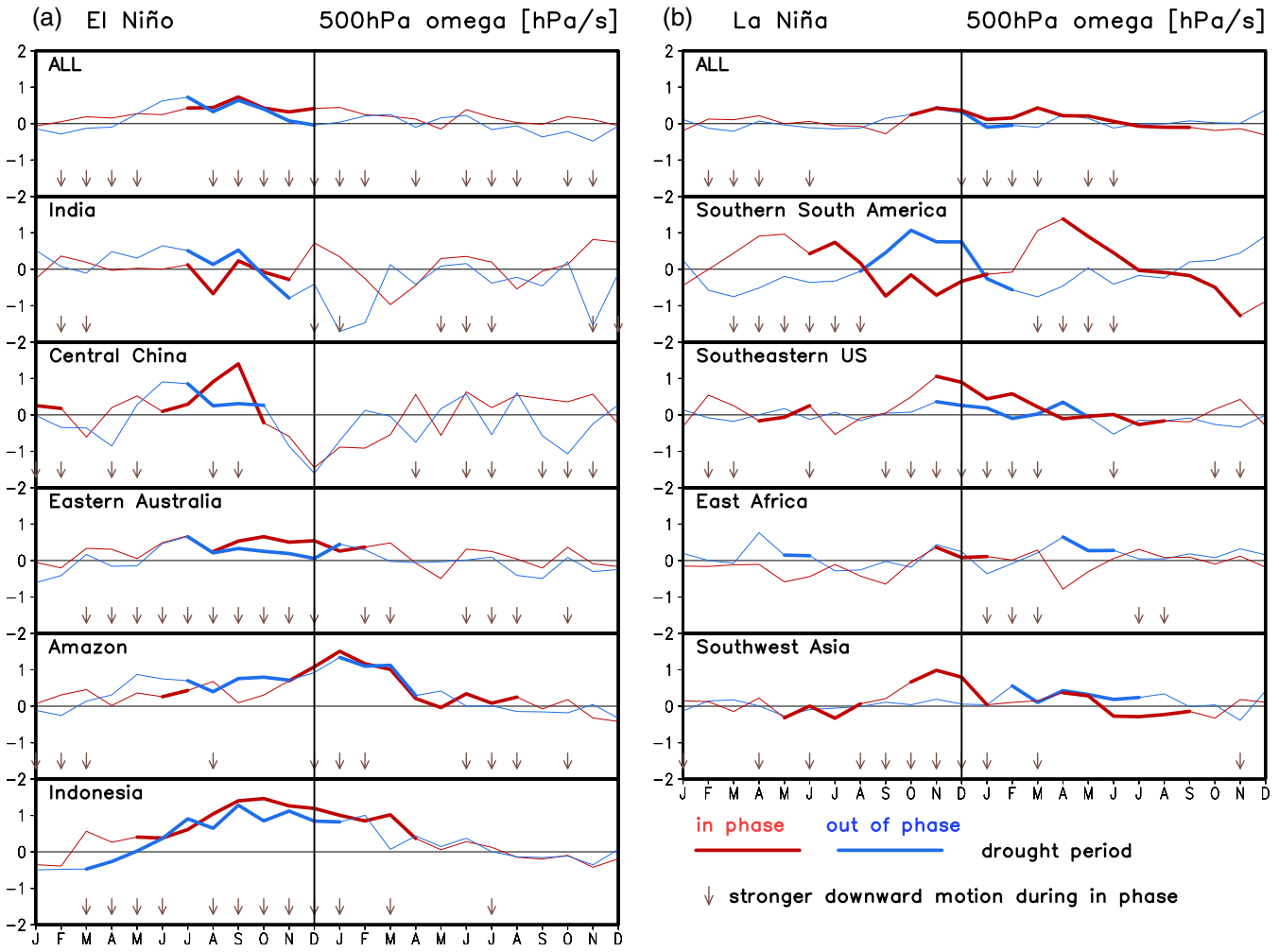

FIGURE 8 Composite time series of the 500 hPa omega (positive: Downward motion) anomalies during the 24-month period of (a) El Niño and (b) La Niña for the in-phase (red line) and out-of-phase (blue line) combinations with PDO. The thick solid lines represent drought period based on SPEI3 < −0.84 (see Figure S7). Brown downward arrows indicate that the downward motion during the in phase years is stronger than the out-of-phase years [Colour figure can be viewed at wileyonlinelibrary.com]

teleconnection patterns, which may in turn bring distinct changes in regional P and PET. In this respect, we examine regional responses of P and PET corresponding to ENSO events under different PDO phases. To be consistent with the SPEI calculation, cumulative anomalies of P and PET at 1–12 month time scales are constructed. Figure 7 compares the evolution of P and PET anomalies at various time scales obtained from the four sub-composites of ENSO and PDO, averaged over corresponding El Niño and La Niña hotspots. It is evident that change in P is the most important driver that accounts for many negative SPEIs although the signals display some regional differences in its magnitude and timing. For example, the intensification of drought when ENSO occurs in phase with PDO is mainly caused by reduction in P over most drought hotspots (Figures S10 and S11 for each hotspot results), explaining more than 50% of total reduction in P-PET. When El Niño occurs in the warm PDO phase, significant negative anomalies of 1-month P is recorded from late spring (May) of the previous year, playing a precursor role of ENSO-induced droughts (Figure 7a). These negative anomalies persist over 1 year, inducing stronger drought conditions at longer time scale. Upon the out-of-phase condition, the El Niño-induced drying signal cannot be detected until September of previous year and lasts only for several months to next August at 12-month time scales (Figure 7b). In cases of La Niña hotspots, the well-defined drying responses emerge commonly around November–December of the previous year for both cold and warm PDO (Figure 7d,e). Although below-normal precipitation is observed over similar periods, drought intensity gets stronger during La Niña/cold PDO combination from spring to fall. This distinct response in P reasonably explains delayed withdrawals of the La Niña-induced droughts during the cold PDO. The composite difference

patterns (Figure 7c,f) clearly show the asymmetric influence of the PDO polarity on P during El Niño and La Niña, consistent with SPEI results (Figure 4e,f).

The results also indicate that PET partly contributes to intense droughts when ENSO and PDO are in phase conditions, particularly for La Niña hotspots (Figure 7, right panel). El Niño-induced PET amplification effect during warm PDO is found to be weak, with significant PET increases identifiable only over central China (Figure S10). In contrast, a stronger contribution of PET increase to drought intensification is observed for all La Niña hotspots except Southwest Asia (Figure S11). In particular, PET contribution plays an important role in maintaining the dry conditions over southern South America and southeastern United States.

In order to reaffirm atmospheric circulation patterns that drive ENSO-PDO combined effects on droughts (Wang *et al.*, 2014), we examine composite patterns of 500 hPa vertical velocity (omega) averaged over hotspots during the 24-month period of ENSO events (Figure 8). Here, drought periods are determined based on 3-month SPEIs (< -0.84, Figure S7) to better capture the ENSO-induced circulation responses (Vicente-Serrano *et al.*, 2011). Results show that several hotspots such as central China, eastern Australia, and Indonesia for El Niño and southeastern United States and southwest Asia for La Niña experience intensified downward motion (positive omega) when they occur in phase with PDO and vice versa, supporting previous findings (Vicente-Serrano *et al.*, 2011; Wang *et al.*, 2014). It is interesting to see that these circulation responses occur with different timing between El Niño and La Niña hotspots, in accord with the corresponding drought evolutions (Figure S7). Composite evolutions of 200 hPa convergence anomalies exhibit similar results (not shown), indicating that different phases of PDO systematically modulate the ENSO teleconnection patterns.

3.4 | Role of El Niño types in drought responses

There are diverse "ENSO flavours" (Trenberth and Smith, 2006; Johnson, 2013) and the associated teleconnections can be modulated by PDO in a different way (cf. Yeh *et al.*, 2018; Zhao *et al.*, 2019; Rao *et al.*, 2019a). In this respect, we have briefly examined which El Niño types (EP El Niño vs. CP El Niño) are more affected by different PDO phases using available samples. As mentioned above, as there was no CP El Niño event before 1950, a recent period of 1950–2015 was considered here. There were six CP El Niño events (Table 1, underlined years) with half of them occurring under the warm PDO and the other half under the cold PDO. During the same period, there were 10 EP El Niño events with four under warm PDO and six under cold PDO. We redo our analysis using these CP and EP El Niño events and examine drought responses in comparison with those from all El Niño years. Note that this result should be interpreted with caution due to small sample size. The spatial pattern of SPEI12 composites (Figure 9) show that drought response during EP El Niño (Figure 9b) is very similar to that from all El Niño

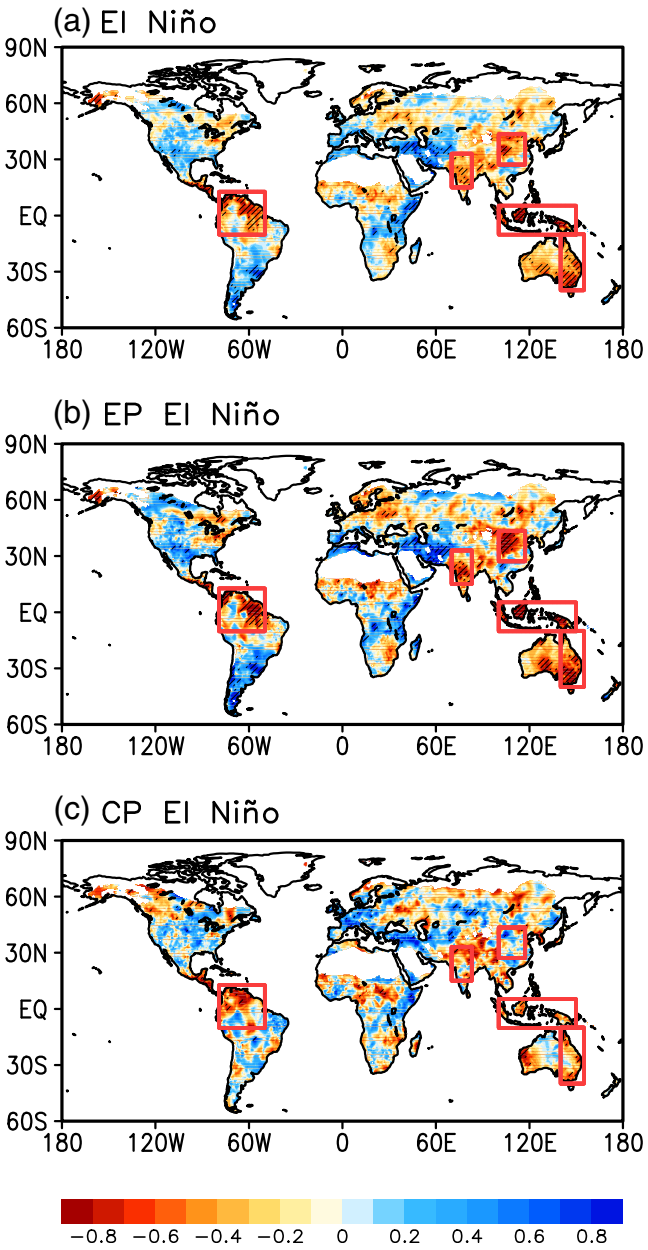

FIGURE 9 Composite of the DJF detrended SPEI12 for (a) El Niño, (b) EP El Niño, and (c) CP El Niño during 1950–2015 (see Table 1). The hatching indicates significant results at 10% level according to a two-tailed Student's *t*-test [Colour figure can be viewed at wileyonlinelibrary.com]

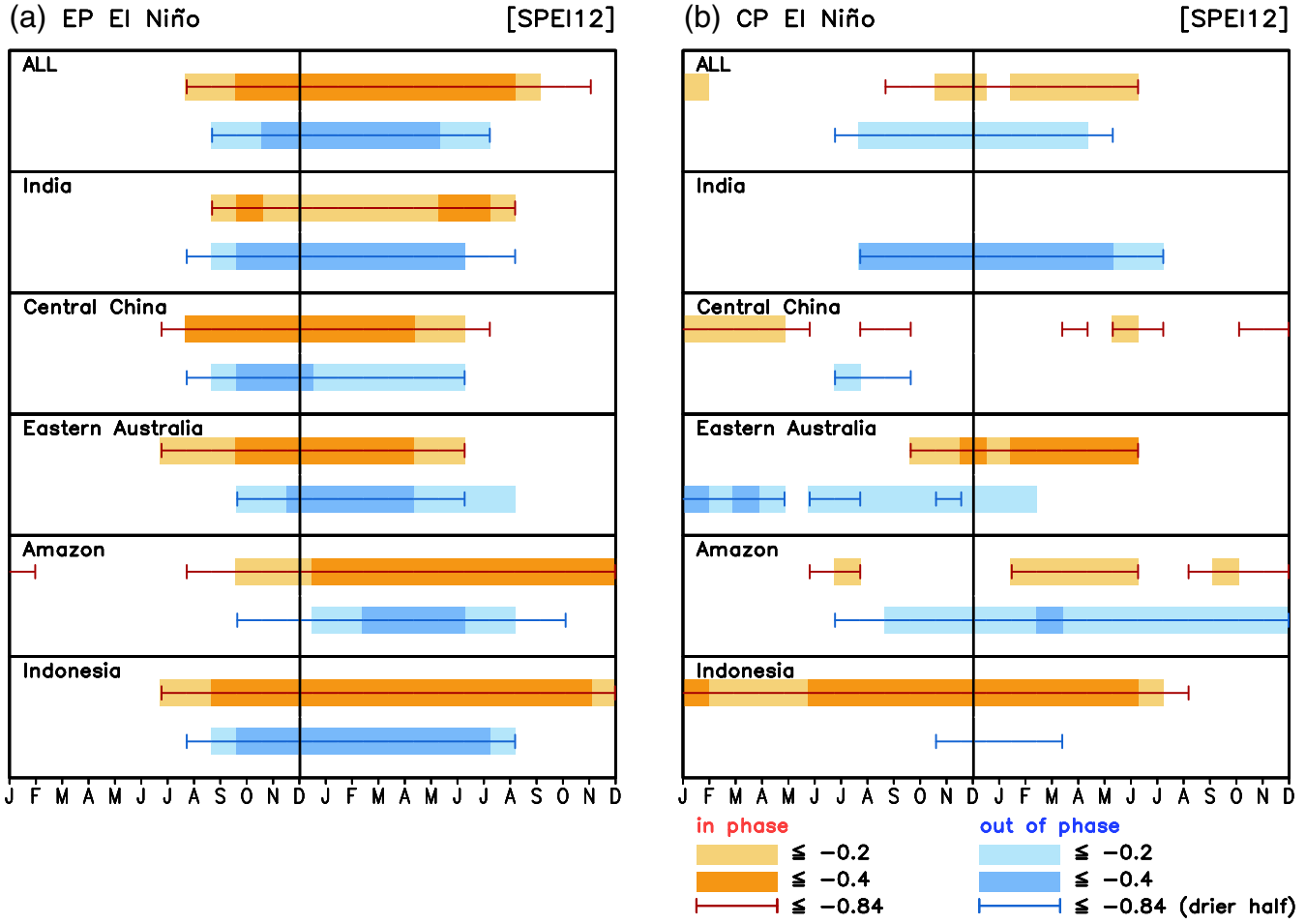

FIGURE 10 Same as Figure 5 but for (a) EP El Niño and (b) CP El Niño during 1950–2015 [Colour figure can be viewed at wileyonlinelibrary.com]

(Figure 9a), with significant decreases in SPEI12 well identified in all five hotspots. In contrast, CP El Niño events (Figure 9c) exhibit much weaker drought responses than EP El Niño. In particular, eastern Australia and Amazon have much smaller area of negative SPEIs, and India and central China even have no drought signal on average during CP El Niño.

To examine PDO modulation effects on different El Nino types, drought durations over five hotspots are compared between warm and cold PDOs for EP and CP El Niño events, respectively. Figure 10 shows the onset and withdraw of drought based on SPEI12 for hotspot averages and individual hotspots. Overall, the strength and duration of droughts during EP El Niño resemble those from all El Niño events (Figure S12), also consistent with composite patterns (Figure 9). In contrast, drought becomes much weaker and shorter during CP El Niño with a larger difference across hotspots. A comparison of drought responses between the warm and cold PDO reveals that overall weakened and shortened drought in the cold PDO is clearly observed during EP El Niño, which is not the case for CP El Niño. In particular, drought starts earlier over central China, Amazon, and Indonesia and ends later over India, Amazon, and Indonesia when EP El Niño occurs in combination with the warm PDO. PDO influence on CP El Niño-induced drought is very uncertain as indicated by a large difference among hotspots. One interesting feature is that India and Amazon tend to experience longer drought when CP El Nino occurs with cold PDO, which suggests that there might be a different ENSO-PDO combined impact on drought, depending on El Niño types. Again, considering small sample size, this result remains inconclusive, warranting further investigation based on relevant model experiments.

4 | SUMMARY AND CONCLUSIONS

ENSO has been demonstrated as a primary cause of droughts in many part of the world on the interannual

time scale and recent studies suggested a possible modulation of ENSO-induced drought patterns by PDO. This research further examined responses of global and regional drought characteristics including magnitude, timing and duration under different ENSO-PDO combinations. A multi-scalar drought index of SPEI was utilized at different time scales of drought (1–12 months) to better present the evolution of drought under different ENSO-PDO combinations. In addition, we investigated the possible mechanism accounting for the asymmetric influences of El Niño and La Niña events on droughts under different PDO phases by comparing Niño3.4 SST evolutions and analysing the relative contribution of P and PET to SPEI changes. Also, PDO modulation impacts on different El Niño types are examined.

The composite analyses of 12-month time scale reveal the intensification and area expansion of droughts at all hotspots when ENSO is in phase with PDO. During the out-of-phase PDO, ENSO-induced drought is damped or even disappears in some regions. These findings are in good agreement with the previous results based on the sc_PDSI data (Wang *et al*., 2014). Furthermore, analyses of hydrological drought evolution during 24 months of ENSO events exhibit similar features over all drought hotspots with longer duration in the in-phase conditions resulted from earlier drought onset and later drought withdrawal. However, actual timing or duration of drought varies significantly between El Niño and La Niña and also among regions. Interestingly, during the in-phase combination with PDO, La Niña tends to delay the drought withdrawal until the end of event year whereas El Niño tends to advance the drought onset up to the early summer of previous year.

To understand mechanisms behind the asymmetric modulation of ENSO-induced drought by PDO, we analysed SST anomaly composites. Results show that El Niño itself starts earlier and ends later during the warm PDO phase, partly explaining the extended droughts over the El Niño hotspots. However, there is no distinct difference in the timing and duration of La Niña event under different PDO phases. This asymmetry in the atmospheric response to El Niño and La Niña SST anomalies is consistent with previous studies (Hoerling *et al*., 1997, 2001; Rao and Ren, 2016; Okumura *et al*., 2017b; Zhao *et al*., 2019). Additional analyses of P and PET show the dominant role of precipitation decrease in determining drought characteristics over many hotspots, resembling drought propagation patterns during the 24-month period of ENSO event under different PDO phases. In addition, substantial increase in PET is found to contribute partly to the drier conditions over the two La Niña hotspots of southern South American and southeastern United States. Atmospheric circulation composites indicate the intensified downward motion over several hotspots when ENSO occurs in phase with PDO, supporting previous studies. Furthermore, a comparison of drought responses between El Niño types indicates that the PDO modulation of El Niño-induced drought occurs mainly through EP El Niño with unclear and much weaker response during CP El Niño.

ENSO is the most prominent mode of climate variability on Earth, and our results on the PDO modulation of ENSO-induced drought characteristics have important implications. Since many regions in the world are expected to be vulnerable to prolonged droughts under decadal variability and global warming (Vicente-Serrano *et al*., 2020 and references therein), findings in this research will be useful to improve long-term predictions of drought by helping to construct early warning and monitoring systems. Detailed analyses of historical drought events provide more opportunities in drought management and mitigation (Vicente-Serrano *et al*., 2010; IPCC, 2012).

ACKNOWLEDGEMENTS

The authors thank Scott Power for useful comments on our initial results and two anonymous reviewers for their constructive comments on our manuscript. This work was supported by the Korea Meteorological Administration Research and Development Program under Grant KMI 2018-03610 and by a National Research Foundation of Korea (NRF) grant funded by the South Korean government (MSIT) (Grant 2017R1A2B2008951).

ORCID

Seung-Ki Min https://orcid.org/0000-0002-6749-010X
Yeon-Hee Kim https://orcid.org/0000-0003-0233-1690

REFERENCES

Andreoli, R.V. and Kayano, M.T. (2005) ENSO-related rainfall anomalies in South America and associated circulation features during warm and cold Pacific decadal oscillation regimes. *International Journal of Climatology*, 25, 2017–2030. https://doi.org/10.1002/joc.1222.

Ashcroft, L., Karoly, D.J. and Gergis, J. (2014) Southeastern Australian climate variability 1860-2009: a multivariate analysis. *International Journal of Climatology*, 34, 1928–1944. https://doi.org/10.1002/joc.3812.

Barker, L.J., Hannaford, J., Chiverton, A. and Svensson, C. (2016) From meteorological to hydrological drought using standardised indicators. *Hydrology and Earth System Sciences*, 20, 2483–2505. https://doi.org/10.5194/hess-20-2483-2016.

Barlow, M., Zaitchik, B., Paz, S., Black, E., Evans, J. and Hoell, A. (2016) A review of drought in the Middle East and Southwest Asia. *Journal of Climate*, 29, 8547–8574. https://doi.org/10.1175/jcli-d-13-00692.1.

Brönnimann, S. (2007) Impact of El Niño-Southern Oscillation on European climate. *Reviews of Geophysics*, 45, 181–197. https://doi.org/10.1029/2006rg000199.

Carrao, H., Singleton, A., Naumann, G., Barbosa, P. and Vogt, J. (2014) An optimized system for the classification of meteorological drought intensity with applications in drought frequency analysis. *Journal of Applied Meteorology and Climatology*, 53, 1943–1960.

Coghlan, A. (2011) La Niña behind East Africa's drought. *New Scientist*, 211, 12. https://doi.org/10.1016/s0262-4079(11)61611-4.

Dai, A., Fyfe, J.C., Xie, S.-P. and Dai, X. (2015) Decadal modulation of global surface temperature by internal climate variability. *Nature Climate Change*, 5, 555–559. https://doi.org/10.1038/nclimate2605.

Diaz, H.F., Hoerling, M.P. and Eischeid, J.K. (2001) ENSO variability, teleconnections and climate change. *International Journal of Climatology*, 21, 1845–1862. https://doi.org/10.1002/joc.631.

Ficklin, D.L., Maxwell, J.T., Letsinger, S.L. and Gholizadeh, H. (2015) A climatic deconstruction of recent drought trends in the United States. *Environmental Research Letters*, 10, 044009. https://doi.org/10.1088/1748-9326/10/4/044009.

García-Herrera, R., Hernández, E., Barriopedro, D., Paredes, D., Trigo, R.M., Trigo, I.F. and Mendes, M.A. (2007) The outstanding 2004/05 drought in the Iberian Peninsula: associated atmospheric circulation. *Journal of Hydrometeorology*, 8, 483–498. https://doi.org/10.1175/jhm578.1.

Gershunov, A. and Barnett, aTP. (1998) Interdecadal modulation of ENSO teleconnections. *Bulletin of American Meteorololgical Society*, 98, 2715–2725.

Ghebrezgabher, M.G., Yang, T. and Yang, X. (2016) Long-term trend of climate change and drought assessment in the horn of Africa. *Advances in Meteorology*, 2016, 1–12. https://doi.org/10.1155/2016/8057641.

Gu, G., Adler, R.F., Huffman, G.J. and Curtis, S. (2007) Tropical rainfall variability on interannual-to-interdecadal and longer time scales derived from the GPCP monthly product. *Journal of Climate*, 20, 4033–4046. https://doi.org/10.1175/jcli4227.1.

Harris, I., Jones, P.D., Osborn, T.J. and Lister, D.H. (2014) Updated high-resolution grids of monthly climatic observations-the CRU TS3.10 Dataset. *Internatioanl Journal of Climatology*, 34, 623–642. https://doi.org/10.1002/joc.3711.

Hoell, A., Funk, C. and Barlow, M. (2014) La Niña diversity and Northwest Indian Ocean rim teleconnections. *Climate Dynamics*, 43, 2707–2724. https://doi.org/10.1007/s00382-014-2083-y.

Hoerling, M.P., Kumar, A. and Zhong, M. (1997) El Niño, La Niña, and the nonlinearity of their teleconnections. *Journal of Climate*, 10, 1769–1786.

Hoerling, M.P., Kumar, A. and Xu, T. (2001) Robustness of the nonlinear climate response to ENSO's extreme phases. *Journal of Climate*, 14, 1277–1293.

Hoerling, M., Hurrell, J., Eischeid, J. and Philips, A. (2006) Detection and attribution of twentieth-century northern and southern African rainfall change. *Journal of Climate*, 19, 3989–4008.

Hong, C.-C., Wu, Y.-K., Li, T. and Chang, C.-C. (2013) The climate regime shift over the Pacific during 1996/1997. *Climate Dynamics*, 43, 435–446. https://doi.org/10.1007/s00382-013-1867-9.

Hu, Z.-Z. and Huang, B. (2009) Interferential impact of ENSO and PDO on dry and wet conditions in the U.S. Great Plains. *Journal of Climate*, 22, 6047–6065. https://doi.org/10.1175/2009jcli2798.1.

IPCC. (2012) *Managing the risks of extreme events and disasters to advance climate change adaptation*. A Special Report of Working Groups I and II of the Intergovernmental Panel on Climate Change. Cambridge University Press, Cambridge, UK, and New York, NY.

Jimenez-Munoz, J.C., Mattar, C., Barichivich, J., Santamaría-Artigas, A., Takahashi, K., Malhi, Y., Sobrino, J.A. and van der Schrier, G. (2016) Record-breaking warming and extreme drought in the Amazon rainforest during the course of El Niño 2015-2016. *Scientific Reports*, 6, 33130. https://doi.org/10.1038/srep33130.

Johnson, N.C. (2013) How many ENSO flavors can we distinguish? *Journal of Climate*, 26, 4816–4827. https://doi.org/10.1175/jcli-d-12-00649.1.

Kim, J.-W., Yeh, S.-W. and Chang, E.-C. (2013) Combined effect of El Niño-southern oscillation and Pacific decadal oscillation on the east Asian winter monsoon. *Climate Dynamics*, 42, 957–971. https://doi.org/10.1007/s00382-013-1730-z.

Krishnamurthy L, Krishnamurthy V. (2013) *Influence of PDO on South Asian summer monsoon and monsoon-ENSO relation*. COLA Technical Report number: 321.

López-Moreno, J.I., Vicente-Serrano, S.M., Zabalza, J., Beguería, S., Lorenzo-Lacruz, J., Azorin-Molina, C. and Morán-Tejeda, E. (2013) Hydrological response to climate variability at different time scales: a study in the Ebro basin. *Journal of Hydrology*, 477, 175–188. https://doi.org/10.1016/j.jhydrol.2012.11.028.

Manatsa, D., Mushore, T. and Lenouo, A. (2015) Improved predictability of droughts over southern Africa using the standardized precipitation evapotranspiration index and ENSO. *Theoretical and Applied Climatology*, 127, 259–274. https://doi.org/10.1007/s00704-015-1632-6.

Mantua, N.J., Hare, S.R., Zhang, Y., Wallace, J.M. and Francis, R.C. (1997) A Pacific interdecadal climate oscillation with impacts on salmon production. *Bulletin of American Meteorololgical Society*, 78, 1069–1079.

McCabe, G.J., Palecki, M.A. and Betancourt, J.L. (2004) Pacific and Atlantic Ocean influences on multidecadal drought frequency in the United States. *Proceeding of the National Academy of Sciences of the USA*, 101, 4136–4141. https://doi.org/10.1073/pnas.0306738101.

McGree, S., Schreider, S. and Kuleshov, Y. (2016) Trends and variability in droughts in the Pacific islands and Northeast Australia. *Journal of Climate*, 29, 8377–8397. https://doi.org/10.1175/jcli-d-16-0332.1.

McKee, T.B., Doesken, N.J. and Kleist, J. (1993) The relationship of drought frequency and duration to time scales. *Proceedings of the Eighth Conference on Applied Climatology*, *17–22 January*, *Anaheim*, *CA*. Boston, MA: Amerian Meteorological Society, pp. 179–184.

Newman, M., Alexander, M.A., Ault, T.R., Cobb, K.M., Deser, C., di Lorenzo, E., Mantua, N.J., Miller, A.J., Minobe, S., Nakamura, H., Schneider, N., Vimont, D.J., Phillips, A.S., Scott, J.D. and Smith, C.A. (2016) The Pacific decadal oscillation, revisited. *Journal of Climate*, 29, 4399–4427. https://doi.org/10.1175/jcli-d-15-0508.1.

Namias, J., Yuan, X. and Cayan, D.R. (1988) Persistence of North Pacific Sea surface temperature and atmospheric flow patterns. *Journal of Climate*, 1, 682–703. https://doi.org/10.1175/1520-0442(1988)001<0682:PONPSS>2.0.CO;2.

Newman, M., Compo, G.P. and Alexander, M.A. (2003) ENSO-forced variability of the Pacific decadal oscillation. *Journal of Climate*, 16, 3853–3857.

Okumura, Y.M., DiNezio, P. and Deser, C. (2017a) Evolving impacts of multiyear La Niña events on atmospheric circulation and U.S. drought. *Geophyysical Research Letters*, 44, 11614–611623. https://doi.org/10.1002/2017gl075034.

Okumura, Y.M., Sun, T. and Wu, X. (2017b) Asymmetric modulation of El Niño and La Niña and the linkage to tropical Pacific decadal variability. *Journal of Climate*, 30, 4705–4733. https://doi.org/10.1175/jcli-d-16-0680.1.

Palmer, W.C. (1965) *Meteorological droughts*. Department of Commerce, Weather Bureau Research Paper number: 45. p. 58

Papineau, J.M. (2001) Wintertime temperature anomalies in Alaska correlated with ENSO and PDO. *International Journal of Climatology*, 21, 1577–1592.

Pavia, E.G., Graef, F. and Reyes, J. (2006) PDO–ENSO effects in the climate of Mexico. *Journal of Climate*, 19, 6433–6438.

Penalba, O.C. and Rivera, J.A. (2016) Precipitation response to El Niño/La Niña events in southern South America-emphasis in regional drought occurrences. *Advances in Geosciences*, 42, 1–14. https://doi.org/10.5194/adgeo-42-1-2016.

Peng, L., Li, D. and Sheffield, J. (2018) Drivers of variability in atmospheric evaporative demand: multiscale spectral analysis based on observations and physically based modeling. *Water Resources Research*, 54, 3510–3529. https://doi.org/10.1029/2017WR022104.

Peña-Gallardo, M., Vicente-Serrano, S.M., Hannaford, J., Lorenzo-Lacruz, J., Svoboda, M., Domínguez-Castro, F., Maneta, M., Tomas-Burguera, M. and Kenawy, A.E. (2019) Complex influences of meteorological drought time-scales on hydrological droughts in natural basins of the contiguous Unites States. *Journal of Hydrology*, 568, 611–625. https://doi.org/10.1016/j.jhydrol.2018.11.026.

Quintana J. (2000) The drought in Chile and La Niña. *Drought Network News (1994–2001)*, p. 71.

Rao, J. and Ren, R. (2016) Asymmetry and nonlinearity of the influence of ENSO on the northern winter stratosphere: 2. Model study with WACCM. *Journal of Geophysical Research*, 121, 9017–9032.

Rao, J. and Ren, R. (2017) Parallel comparison of the 1982/83, 1997/98, and 2015/16 super El Niños and their effects on the extratropical stratosphere. *Advances in Atmospheric Sciences*, 34, 1121–1133. https://doi.org/10.1007/s00376-017-6260-x.

Rao, J. and Ren, R. (2018) Varying stratospheric responses to tropical Atlantic SST forcing from early to late winter. *Climate Dynamics*, 51, 2079–2096. https://doi.org/10.1007/s00382-017-3998-x.

Rao, J., Garfinkel, C. and Ren, R. (2019a) Modulation of the northern winter stratospheric El Niño–southern oscillation teleconnection by the PDO. *Journal of Climate*, 32, 5761–5783.

Rao, J., Ren, R., Xia, X., Shi, C. and Guo, D. (2019b) Combined impact of El Niño–southern oscillation and Pacific decadal oscillation on the northern winter stratosphere. *Atmosphere*, 10, 211.

Rayner, N.A., Parker, D.E., Horton, E.B., Folland, C.K., Alexander, L.V., Rowell, D.P., Kent, E.C. and Kaplan, A. (2003) Global analyses of sea surface temperature, sea ice, and night marine air temperature since the late nineteenth century. *Journal of Geophysical Research*, 108(D14), 4407. https://doi.org/10.1029/2002jd002670.

Rivera, J. and Penalba, O. (2014) Trends and spatial patterns of drought affected area in southern South America. *Climate*, 2, 264–278. https://doi.org/10.3390/cli2040264.

Rouault, M. (2005) Intensity and spatial extent of droughts in southern Africa. *Geophyysical Research Letters*, 32, L15702. https://doi.org/10.1029/2005gl022436.

Schneider, N. and Cornuelle, B.D. (2005) The forcing of the Pacific decadal oscillation. *Journal of Climate*, 18, 4355–4373. https://doi.org/10.1175/JCLI3527.1.

Sen Roy, S., Goodrich, G.B. and Balling, R.C., Jr. (2003) Influence of El Niño/southern oscillation, Pacific decadal oscillation, and local sea-surface temperature anomalies on peak season monsoon precipitation in India. *Climate Researh*, 25, 171–178.

Spinoni, J., Nausemann, G., Carrao, H., Barbosa, P. and Vogt, J. (2014) World drought frequency, duration, and severity for 1951-2010. *Internatioanl Journal of Climatology*, 34, 2792–2804. https://doi.org/10.1002/joc.3875.

Stan, C., Straus, D.M., Frederiksen, J.S., Lin, H., Maloney, E.D. and Schumacher, C. (2017) Review of tropical-extratropical teleconnections on intraseasonal time scales. *Reviews of Geophysics*, 55, 902–937. https://doi.org/10.1002/2016rg000538.

Sun, Q., Miao, C., AghaKouchak, A. and Duan, Q. (2016) Century-scale causal relationships between global dry/wet conditions and the state of the Pacific and Atlantic oceans. *Geophyysical Research Letters*, 43, 6528–6537. https://doi.org/10.1002/2016gl069628.

Trenberth, K.E. and Hoar, T.J. (1997) El Niño and climate change. *Geophyysical Research Letters*, 24, 3057–3060. https://doi.org/10.1029/97gl03092.

Trenberth, K.E., Caron, J.M., Stepaniak, D.P. and Worley, S. (2002) Evolution of El Niño–southern oscillation and global atmospheric surface temperatures. *Journal of Geophysical Research*, 107(D8), 4065. https://doi.org/10.1029/2000JD000298.

Trenberth, K.E. and Smith, L. (2006) The vertical structure of temperature in the tropics: different flavors of El Niño. *Journal of Climate*, 19, 1956–4970.

Trenberth, K.E., Dai, A., van der Schrier, G., Jones, P.D., Barichivich, J., Briffa, K.R. and Sheffield, J. (2014) Global warming and changes in drought. *Nature Climate Change*, 4, 17–22. https://doi.org/10.1038/nclimate2067.

Vicente-Serrano, S.M., Beguería, S. and López-Moreno, J.I. (2010) A multiscalar drought index sensitive to global warming: the standardized precipitation evapotranspiration index. *Journal of Climate*, 23, 1696–1718. https://doi.org/10.1175/2009jcli2909.1.

Vicente-Serrano, S.M., López-Moreno, J.I., Gimeno, L., Nieto, R., Morán-Tejeda, E., Lorenzo-Lacruz, J., Beguería, S. and Azorin-Molina, C. (2011) A multiscalar global evaluation of the impact of ENSO on droughts. *Journal of Geophysical Research*, 116, D20109. https://doi.org/10.1029/2011jd016039.

Vicente-Serrano, S.M., Gouveia, C., Camarero, J.J., Beguería, S., Trigo, R., López-Moreno, J.I., Azorín-Molina, C., Pasho, E., Lorenzo-Lacruz, J., Revuelto, J., Morán-Tejeda, E. and Sanchez-Lorenzo, A. (2013) Response of vegetation to drought time-scales across global land biomes. *Proceedings of the National Academy of Sciences of the United States of America*, 110(1), 52–57. https://doi.org/10.1073/pnas.1207068110.

Vicente-Serrano, S.M., McVicar, T.R., Miralles, D.G., Yang, Y. and Tomas-Burguera, M. (2020) Unraveling the influence of atmospheric evaporative demand on drought and its response to climate change. *WIREs Climate Change*, 11(2), e632. https://doi.org/10.1002/wcc.632.

Wang, L., Chen, W. and Huang, R. (2008) Interdecadal modulation of PDO on the impact of ENSO on the east Asian winter monsoon. *Geophysical Research Letters*, 35, L20702. https://doi.org/10.1029/2008gl035287.

Wang, S., Huang, J., He, Y. and Guan, Y. (2014) Combined effects of the Pacific decadal oscillation and El Niño-southern oscillation on global land dry-wet changes. *Scientific Reports*, 4, 6651. https://doi.org/10.1038/srep06651.

Wells, N., Goddard, S. and Hayes, M.J. (2004) A self-calibrating Palmer drought severity index. *Journal of Climate*, 17, 2335–2351. https://doi.org/10.1175/1520-0442(2004)017<2335:ASPDSI>2.0.CO;2.

Wu, X. and Mao, J. (2016) Interdecadal modulation of ENSO-related spring rainfall over South China by the Pacific decadal oscillation. *Climate Dynamics*, 47, 3203–3220.

Wu, X. and Mao, J. (2017) Interdecadal variability of early summer monsoon rainfall over South China in association with the Pacific decadal oscillation. *International Journal of Climatology*, 37, 706–721.

Wu, X. and Mao, J. (2018) Spatial and interannual variations of spring rainfall over eastern China in association with PDO–ENSO events. *Theoretical and Applied Climatology*, 134, 935–953.

Xiao, M., Zhang, Q. and Vijay, S. (2015) Influences of ENSO, NAO, IOD and PDO on seasonal precipitation regimes in the Yangtze River basin, China. *International Journal of Climatology*, 35, 3556–3567.

Yeh, S.-W., Cai, W., Min, S.-K., McPhaden, M.J., Dommenget, D., Dewitte, B., Collins, M., Ashok, K., An, S.-I., Yim, B.-Y. and Kug, J.-S. (2018) ENSO atmospheric teleconnections and their response to greenhouse gas forcing. *Reviews of Geophysics*, 56, 185–206. https://doi.org/10.1002/2017RG000568.

Yeh, S.-W., Kug, J.-S., Dewitte, B., Kwon, M.-H., Kirtman, B.P. and Jin, F.-F. (2009) El Niño in a changing climate. *Nature*, 461, 511–514. https://doi.org/10.1038/nature08316.

Zanchettin, D., Franks, S.W., Traverso, P. and Tomasino, M. (2008) On ENSO impacts on European wintertime rainfalls and their modulation by the NAO and the Pacific multi-decadal variability described through the PDO index. *International Journal of Climatology*, 28, 995–1006.

Zhao, X., Rao, J. and Mao, J. (2019) The salient differences in China summer rainfall response to ENSO: phases, intensities and flavors. *Climate Research*, 78(1), 51–67.

Zou, Y., Macau, E.E.N., Sampaio, G., Ramos, A.M.T. and Kurths, J. (2015) Do the recent severe droughts in the Amazonia have the same period of length? *Climate Dynamics*, 46, 3279–3285. https://doi.org/10.1007/s00382-015-2768-x.

SUPPORTING INFORMATION

Additional supporting information may be found online in the Supporting Information section at the end of this article.

How to cite this article: Nguyen P-L, Min S-K, Kim Y-H. Combined impacts of the El Niño-Southern Oscillation and Pacific Decadal Oscillation on global droughts assessed using the standardized precipitation evapotranspiration index. *Int J Climatol*. 2020;1–18. https://doi.org/10.1002/joc.6796